Multicomponent trace-gas analysis by three intracavity photoacoustic cells in a CO laser: observation of anaerobic and postanaerobic emission of acetaldehyde and ethanol in cherry tomatoes

Frans G. C. Bijnen, Hanna Zuckermann, Frans J. M. Harren, and Jörg Reuss

Three serial photoacoustic cells are employed within the cavity of a liquid-nitrogen-cooled CO laser to monitor on-line trace-gas concentrations. Multicomponent gas analysis is performed on sequential repetitive measurements of ethylene, acetaldehyde, CO_2, ethanol, and H_2O. To demonstrate the high sensitivity of the laser photoacoustic detector for the biologically interesting gases, acetaldehyde (0.1-parts per billion in volume detection limit) and ethanol (10 parts per billion in volume), we follow the time-dependent release by cherry tomatoes during changing aerobic–anaerobic conditions. © 1998 Optical Society of America

OCIS codes: 300.0300, 010.1280, 140.4130, 280.1120, 300.6360, 300.6430.

1. Introduction

Sensitive multicomponent trace-gas analysis is required to study complex processes in atmospheric chemistry,[1] breath analysis,[2] or plant physiology.[3] Gas chromatography offers the possibility to perform this analysis; however, incubation periods are often required to accumulate gases before injection of gas samples into the gas chromatograph, excluding on-line measurements. Spectroscopic detection allows one to perform on-line multicomponent gas analysis by various techniques.[4] Next to these the recently developed method of cavity ring-down spectroscopy also enables the determination of trace-gas concentrations at levels of parts per billion in volume and even parts per trillion in volume.[5]

Photoacoustic spectroscopy has already been shown to yield extreme sensitivity.[6,7] However, the selectivity of a spectroscopic detection method, when applied to a mixture of gas components, may be hampered owing to spectral overlap of the molecular gases. Earlier multicomponent studies were per-

formed that employed a CO_2 laser in combination with photoacoustics.[8,9] Matrix manipulation permitted the determination of the concentrations of different gas components. Here we present a liquid-nitrogen-cooled CO laser with a larger tuning range ($1250–2080$ cm^{-1}) in comparison with a CO_2 laser ($900–1100$ cm^{-1}); therefore more trace gases can be discriminated. A problem with using the CO laser is water vapor that has a strong absorption band in this wavelength region and often shows interference with trace-gas components to be determined.

A cw CO laser cooled to 265 K was employed previously in a photoacoustic arrangement to monitor multicomponent car exhaust gases.[10] Multiline laser emission and water-vapor absorption caused interference and required a dual-beam arrangement with a reference system. In contrast with the 265-K-operated CO laser, our liquid-nitrogen (77 K) version shows single-line operation.[11] Furthermore, by proper gas handling we reduced perturbing wall-sticking and degassing effects from gaseous molecules. We performed multicomponent analysis by sequentially measuring the absorption signal on various laser lines and analyzing the obtained data by means of a matrix method that leads to concentrations of the individual gases in the mixture. Along with spectral selection, trapping of gases with a low vapor pressure by freezing was used.

The developed detector is applied to measure trace-gas emission of cherry tomatoes during aerobic and
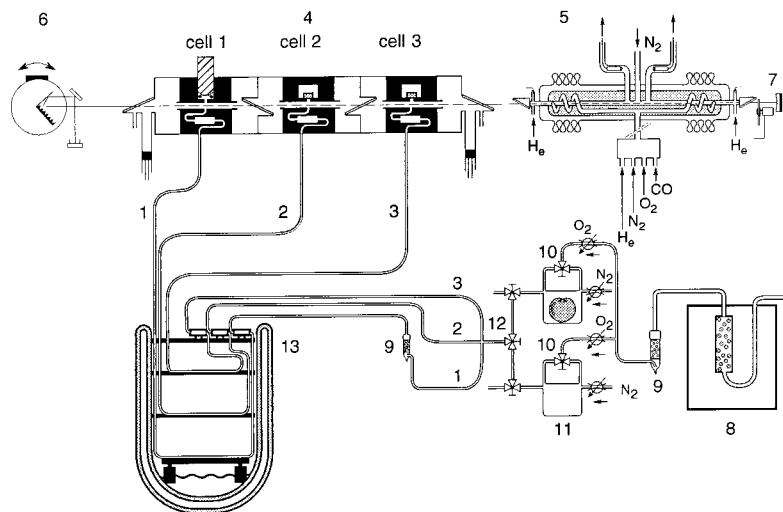
Fig. 1. Detection setup: 1, 2, and 3, trace-gas flows; 4, triple photoacoustic cell; 5, liquid-nitrogen-cooled CO laser; 6, grating to select the appropriate transition; 7, chopper; 8, catalyst to remove hydrocarbons; 9, KOH scrubber to remove CO_2; 10, switching valve for (an)aerobic conditions; 11, cuvettes, one containing a tomato, the other empty as a reference; 12, switching valve to select the cuvette; 13, cooling trap.

anaerobic conditions. During long-term storage of fruit and vegetables reduced oxygen levels are used in modified atmospheric conditions ($<2\%$ O_2, N_2, 5% CO_2 at 5 °C). However, changes in fruit metabolism during and after storage may give rise to the induction of fermentation, tissue damage, and deterioration of fruit. It has been estimated that the worldwide loss amounts to 25–40%.[12] To study the process of deterioration of the fruit, we applied our laser photoacoustic detector to the measurement of the trace-gas emission of tomatoes. The setup allows us to monitor on-line the dynamic changes in the metabolism when the fruit switches from (aerobic) respiration to (anaerobic) fermentation, which are reflected in the emission of CO_2, C_2H_4, and the fermentative metabolites ethanol and acetaldehyde.

2. CO Laser

The liquid-nitrogen-cooled CO laser was described in detail earlier.[13] Here we limit ourselves to a brief description of the setup (Fig. 1) including some improvements.

Laser operation was obtained between 1260 and 2000 cm^{-1} on 250 lines with an intracavity laser power as high as 40 W (at 1920 cm^{-1}). In the long-wavelength region of the emission spectrum many lasing transitions could be sustained at an intracavity power of 1 W. The overall cavity length of the CO laser was increased from 2.2 to 3 m to accommodate the triple photoacoustic cell (900-mm length) and a surrounding acoustic-shielding box.

Multicomponent measurements involve repeated switching between previous chosen laser lines by the tuning of the angle of a Littrow-mounted grating. Simultaneously with the photoacoustic signal, the laser power is monitored at the zero-order outcoupling of the grating. Normally, the concentration of a trace gas is proportional to the ratio of the photoacoustic signal and the intracavity laser power. However, when the grating was somewhat shifted from its optimal position for maximum laser power, we observed that the above ratio for the background

and for the water-vapor signal was not constant. This nonlinear dependence of the photoacoustic signal on the laser power was probably due to the heating of the acoustic resonator wall by higher-order TEM modes of the laser beam. We drastically improved this situation by replacing the $R = 10$ m (radius of curvature) end mirror with an $R = 5$ m mirror in combination with an iris, thus favoring the TEM_{00} mode. The introduction of the iris between the triple cell and the laser tube resulted in an approximately 5% power loss, but the photoacoustic-signal–intracavity-laser-power ratio remained constant over a grating angle change of 0.02°, which is well within the reproducibility of the stepper motor used to tune the grating.

For long-term operation (a few days) of the CO laser, replenishment of the liquid-nitrogen-cooling reservoir surrounding the laser tube was automated by monitoring the level of liquid nitrogen at three heights inside the reservoir. The middle sensor indicated refilling; the upper sensor stopped refilling; and the lower temperature sensor indicated switching to a new, full external liquid-nitrogen container. In this way we could operate the laser for a week. However, operation of the laser could not be extended more since the exit toward the pump became obstructed with solid CO_2 ice, increasing the pressure above the operational value.

3. Triple Photoacoustic Cell

As part of the experimental arrangement the triple cell is shown in Fig. 1. The three photoacoustic cells in the series are separated by nickel-coated brass plane walls of 5-mm thickness supporting Brewster windows. To suppress the in-phase signal caused by window absorption, windows and resonators are separated by buffers with a length of 75 mm ($=\lambda/4$, where λ is the acoustical wavelength) and a radius of 60 mm.[14] Note that the resonators partly (35 mm) enter into the buffer volumes, thus reducing the actual distance between the end of the resonators and the Brewster windows to 40 mm (Fig. 1). The ad-

vantage is a shorter photoacoustic cell; extracavity experiments showed that the suppression of the window signal in this design is comparable with earlier designs.[14] One Bruel and Kjaer (B&K) microphone (B&K type 4179, cell 1) and two Knowless microphones (EK-3024 type, cells 2 and 3) were employed. The three different resonators are described in detail elsewhere[13]: a copper resonator with a polished gold coating (cell 1), a polished brass resonator (cell 2), and a polished stainless-steel resonator (cell 3).

Only one chopper was used, and therefore the resonance frequencies of the cells had to be equalized. The resonance frequency was strongly affected by the 1-in. (2.54-cm) membrane of the B&K condenser microphone.[14] To achieve the same resonance frequency the resonator length of cell 1 (138 mm) was therefore 8 mm shorter than those of the other two cells. The remaining differences in resonance frequency were individually corrected, by heating each resonator with a temperature control unit. The temperature sensor and the heater unit were attached directly to the central part of each resonator. An increase of 1 Hz in resonance frequency was obtained by a temperature increase of 0.5 K ($f_{res} \propto \sqrt{T}$). In practice, a temperature difference between 2 and 7 K is needed; the average temperature was maintained at a few degrees above room temperature.

The triple cell was constructed as a composite system from which each part could easily be exchanged. The three central sections were made of aluminum in which three photoacoustic resonators were centered. Additional holes toward the center of each block perpendicular to the direction of the resonator allowed the positioning of the microphone, the trace-gas inlet, and the temperature control unit. Two holes in the resonator itself permitted the connection of the microphone and the trace-gas inlet to the inner volume. The connections were sealed by O rings to prevent acoustic leakage. The trace-gas inlet contained one notched filter section to decrease external noise.[14] The buffer volumes were constructed of plain 18-mm-thick steel pipe. The buffers of cells 1 and 3 were closed by 20-mm-thick aluminum Brewster window holders containing a length-tunable air column.[14] The inner wall of the buffers was polished and coated with nickel to reduce adsorption of water vapor on the wall. For the same reason all applied O rings were made of Viton. Rubber vibration dampers suppressed the in-phase mechanical vibrations generated by the chopper with Invar rods as intermediates. However, at acoustic resonance there still remained an in-phase constant background signal of 0.5 µPa at the same level as the noise (0.5 µPa/$\sqrt{\text{Hz}}$) of cell 1.

The noise level of the arrangement was improved by a factor of 4 in comparison with the earlier setup that contained only one photoacoustic cell (2 µPa/$\sqrt{\text{Hz}}$).[13] This was due mainly to the heavier construction of the triple cell (50-kg weight). The ultimate (Brownian) noise level was not yet reached (0.2 µPa/$\sqrt{\text{Hz}}$).[13] Contrary to expectations, the improved noise reduction did not lead to a lower detection limit; the increased background level counter-

acted the improved noise situation. Compared with the single intracavity cell, the constant background signal was 1 order of magnitude higher for the triple-cell arrangement (cell 1, 120 µPa/W; cell 2, 200 µPa/W; cell 3, 900 µPa/W). The increased number of Brewster windows (from two to four) induced additional scattering of laser light and, in combination with the increased length, increased wall absorption. Note that the difference in background signal between the three cells was due to the different absorption and heat conduction properties of the wall materials.[13]

4. Absorption Coefficients

The described setup was employed to make a survey of the absorption coefficients on selected CO laser lines of the biologically interesting gases ethylene, acetaldehyde, CO_2, ethanol, and H_2O (Table 1). In addition to these, a complete set of other gases will appear in a future publication. By measuring the absorption spectra of these gases, we observed no phase shifts in the photoacoustic signals, i.e., we could observe no delay in the generation of the photoacoustic signal compared with the modulated laser beam. This effect is known as kinetic cooling and is preferentially observed for atmospheric CO_2 absorption at CO_2 laser lines.[15] To determine the absorption coefficients, we diluted the gases in a buffer gas of N_2 and N_2/O_2 (air ratio) at various concentrations depending on their partial vapor pressure and absorption strength. Within the given errors (Table 1) no effect could be observed of the slightly different collisional-broadening coefficients from the buffer gases on the absorption strength of the gases.

The intracavity power at all laser lines needed to be determined since the zero-order reflection of the grating is wavelength dependent. For this the 100% reflecting mirror was replaced by a 10% outcoupling mirror; the wavelength-dependent transmission curve of the latter was determined by an infrared spectrometer. In this way the intracavity power could be correlated with the extracavity laser power. For the measurements of the fingerprint spectra the 100% reflecting mirror was repositioned. The constants of the photoacoustic cells were determined by an extracavity arrangement with a CO_2 laser at the 10P14 line and with a calibrated mixture of 1.2 ppmv of ethylene in N_2 flowing through the cells.[6] Trace gas mixtures were obtained by mixing pure gases (or vapor pressures at room temperature) with N_2 to levels ranging from 1 ppmv to 1%. With an unchanged experimental arrangement the reproducibility is affected only by the error in the concentration of the gas mixture that was used for calibration.

5. Multicomponent Analyses

For a multicomponent analysis of a gas mixture the CO laser is tuned to L laser lines. For the analyses it is preferred to obtain an overdetermined system $G < L$, where G is the number of gases and L is the number of laser lines; in this way more information can be obtained from the gas mixture, resulting in

Table 1. Selected CO Laser Lines and Absorption Coefficients for Several Gases

Laser Line $P(J'')_{v''}$	Wavelength (cm^{-1})	C_2H_4 atm^{-1} cm^{-1}	Acetaldehyde atm^{-1} cm^{-1}	CO_2 atm^{-1} cm^{-1} $\times$ 10^{-6}	Ethanol atm^{-1} cm^{-1}	H_2O atm^{-1} cm^{-1}
$P(10)_{30}{}^a$	1352.68291	$(12.9 \pm 0.6) \times 10^{-4}$	8.0 ± 0.4	76 ± 3	0.541 ± 0.016	$(17 \pm 2) \times 10^{-4}$
$P(9)_{30}{}^a$	1355.78822	$(17.7 \pm 0.5) \times 10^{-4}$	4.08 ± 0.18	19 ± 4	0.58 ± 0.03	$(20 \pm 3) \times 10^{-4}$
$P(8)_{30}$	1358.85980	$(9.4 \pm 0.2) \times 10^{-4}$	5.7 ± 0.2	134 ± 4	0.79 ± 0.02	$(35 \pm 3) \times 10^{-4}$
$P(7)_{27}$	1434.16033	0.122 ± 0.003	2.71 ± 0.12	4.3 ± 0.2	0.52 ± 0.03	$(118 \pm 3) \times 10^{-4}$
$P(12)_{26}{}^a$	1442.15056	0.185 ± 0.008	4.3 ± 0.2	5.4 ± 1.1	0.60 ± 0.03	$(47 \pm 3) \times 10^{-4}$
$P(11)_{26}{}^a$	1445.46151	1.02 ± 0.03	3.9 ± 0.2	4.9 ± 0.7	0.58 ± 0.01	$(47 \pm 2) \times 10^{-4}$
$P(8)_{25}{}^a$	1479.43785	0.305 ± 0.012	1.05 ± 0.05	2.2 ± 0.6	0.33 ± 0.01	$(78 \pm 2) \times 10^{-4}$
$P(7)_{25}{}^a$	1482.64945	0.304 ± 0.016	1.06 ± 0.05	2.8 ± 0.6	0.35 ± 0.01	$(100 \pm 3) \times 10^{-4}$
$P(11)_{24}{}^a$	1493.81274	$(1490 \pm 1) \times 10^{-4}$	0.86 ± 0.05	1.7 ± 0.4	0.20 ± 0.01	$(142 \pm 2) \times 10^{-4}$
$P(12)_{23}$	1514.68397	$(57.5 \pm 0.7) \times 10^{-4}$	0.59 ± 0.03	3.8 ± 1.1	0.04 ± 0.03	0.090 ± 0.002
$P(11)_{23}$	1518.09931	$(26.8 \pm 1.7) \times 10^{-4}$	0.60 ± 0.03	7.7 ± 0.7	0.09 ± 0.04	0.099 ± 0.003
$P(10)_{23}$	1521.48136	$(28.1 \pm 1.4) \times 10^{-4}$	1.6 ± 0.2	$<1^b$	0.048 ± 0.005	1.36 ± 0.02
$P(11)_{19}$	1616.04057	$(3.7 \pm 0.2) \times 10^{-4}$	0.281 ± 0.017	$<1^b$	0.018 ± 0.005	0.264 ± 0.002
$P(11)_{13}{}^a$	1765.45987	$(41.2 \pm 0.7) \times 10^{-4}$	28 ± 2	2.2 ± 0.2	0.041 ± 0.003	$(106 \pm 6) \times 10^{-4}$
$P(10)_{13}{}^a$	1769.19147	$(18.4 \pm 0.2) \times 10^{-4}$	20.2 ± 1.6	1.7 ± 0.2	0.04 ± 0.01	0.022 ± 0.002
$P(9)_{13}{}^a$	1772.88960	$(65.4 \pm 1.9) \times 10^{-4}$	14.2 ± 1.2	$<1^b$	0.033 ± 0.005	1.37 ± 0.09
$P(8)_{13}$	1776.55411	$(91.4 \pm 0.1) \times 10^{-4}$	9.9 ± 0.8	0.5 ± 0.2	0.03 ± 0.05	$(121 \pm 6) \times 10^{-4}$
$P(12)_{12}{}^a$	1786.85768	$(79.6 \pm 1.1) \times 10^{-4}$	7.2 ± 0.7	0.7 ± 0.2	0.018 ± 0.001	$(54 \pm 3) \times 10^{-4}$
$P(7)_9$	1882.02699	0.119 ± 0.002	0.172 ± 0.012	14.0 ± 0.3	0.023 ± 0.001	$(8.9 \pm 0.5) \times 10^{-4}$
$P(12)_8{}^a$	1888.32251	0.804 ± 0.003	0.120 ± 0.005	20.7 ± 0.3	0.039 ± 0.005	0.019 ± 0.004
$P(9)_7{}^a$	1925.71109	$(837 \pm 1) \times 10^{-4}$	0.084 ± 0.005	49.8 ± 0.4	0.120 ± 0.005	$(11.6 \pm 0.2) \times 10^{-4}$
$P(8)_7$	1929.58571	0.131 ± 0.002	0.083 ± 0.004	47.4 ± 0.3	0.123 ± 0.001	$(1.5 \pm 0.2) \times 10^{-4}$
$P(7)_7{}^a$	1933.42652	$(1620 \pm 3) \times 10^{-4}$	0.090 ± 0.003	1620 ± 3	0.140 ± 0.001	$(42.1 \pm 0.9) \times 10^{-3}$

^{a}These laser lines were selected for the multicomponent analyses.
^{b}Because of the strong water absorption at these laser lines, the absorption coefficient could not be determined accurately.

more accurate results.[8,9] For practical convenience the background signal generated by window absorption and/or resonator-wall absorption is added as a fictive gas component. In the ideal case the measured spectrum $\tilde{\alpha}$ should be equal to the calculated spectrum α.

If the absorption coefficient Σ_{lg} of each gas g at laser line l is known, the total absorption at a laser line α_l is given by

$$\alpha_l = \sum_{g=1}^{G} \Sigma_{lg} \times c_g, \tag{1}$$

where c_g is the concentration of the gas component g. In matrix notation

$$\alpha = \Sigma \cdot \mathbf{c}. \tag{2}$$

If no measurement error at all is specified in the absorption-coefficient matrix Σ and the measured spectrum ($\tilde{\alpha}_l$), the gas concentration $\mathbf{c}$ can be calculated by

$$\mathbf{c} = (\mathbf{\Psi} \cdot \mathbf{\Psi})^{-1} \cdot \mathbf{\Psi}^t \cdot \mathbf{l}, \tag{3}$$

where

$$\Psi_{ij} = \Sigma_{ij}/\alpha_i, \qquad l_i = 1.$$

More general measurement errors must be specified to contribute a realistic error to calculated gas concentrations. The measurement error vector $\Delta\tilde{\alpha}$ (L elements) and an absorption-coefficient error ma-

trix $\Delta\Sigma$($L \times G$ elements) have to be added to $\tilde{\alpha}$ and Σ, respectively.[9] Thus

$$\mathbf{c} = (\mathbf{\Psi}^t \cdot \mathbf{\Psi})^{-1} \cdot \mathbf{\Psi}^t \cdot \boldsymbol{\beta}, \tag{4}$$

where

$$\Psi_{ij} = \Sigma_{ij}/\Delta\alpha_i, \qquad \beta_i = \alpha_i/\Delta\alpha_i.$$

The error in the concentration ($\Delta\mathbf{c}$) has a component that is due to errors in the measurement and a component that is due to errors in the absorption coefficients:

$$(\Delta c_k)^2 = \sum_{i=1}^{G} [(\Delta c^{i0})_k]^2 + \sum_{i=1, j=1}^{G,L} [(\Delta c^{ij})_k]^2. \tag{5}$$

The error that is due to measurement errors is given by

$$(\Delta c^{i0})_k = B_{ki}, \qquad \mathbf{B} = (\mathbf{\Psi}^t \cdot \mathbf{\Psi})^{-1} \cdot \mathbf{\Psi}^t. \tag{6}$$

If no measurement error is specified or if it is set to zero, the contribution of this part to the total uncertainty in the calculated concentrations is ignored. The error caused by uncertainties in the absorption-coefficient matrix is given by[9]

$$(\Delta c^{ij})_k = [(A^{-1})_{kj} \cdot (\tilde{\beta}_i - \beta_i) - (B)_{ki} \cdot c_j] \cdot \Delta\Psi_{i,j}, \tag{7}$$

where

$$\mathbf{A} = \mathbf{\Psi}^t \cdot \mathbf{\Psi}, \quad \Delta\Psi_{ij} = \Delta\Sigma_{ij}/\Delta\alpha_i, \quad \tilde{\beta}_i = \tilde{\alpha}_i/\Delta\alpha_i.$$

The computation of matrix **B** from absorption-coefficient matrix Σ by matrix inversion can suffer from numerical instability. If there were two gases with almost the same absorption profile, the original method would fail because a singular matrix would be inverted. Therefore the alternative method of singular-value decomposition is used to overcome this problem.[16] For this the absorption-coefficient matrix $\Sigma(L \times G)$ can be decomposed into three matrices, $\mathbf{U}(L \times G)$, $\mathbf{W}(G \times G)$, and $\mathbf{V}(G \times G)$, such that

$$\Sigma = \mathbf{U} \cdot \mathbf{W} \cdot \mathbf{V}^t, \qquad (8)$$

where

$$\sum_{i=1}^{L} U_{ik} U_{in} = \delta_{kn} \quad \text{for} \quad 1 \leq k, n \leq G,$$

$$\sum_{j=1}^{G} V_{jk} V_{jn} = \delta_{kn} \quad \text{for} \quad 1 \leq k, n \leq G,$$

$$w_{ij} = w_i \quad \text{if} \quad i = j,$$

$$\text{or} \quad w_{ij} = 0 \quad \text{otherwise.}$$

The matrices $\mathbf{A}^{-1}$ and $\mathbf{B}$ can be computed from $\mathbf{U}$, $\mathbf{V}$, and $\mathbf{W}$ by

$$\mathbf{B} = \mathbf{V} \cdot \mathbf{W}^{-1} \cdot \mathbf{U}^t, \qquad (9)$$

where

$$(W^{-1})_{ij} = \frac{1}{W_{ii}} \quad \text{if} \quad i = j, \quad (W^{-1})_{ij} = 0 \quad \text{otherwise,}$$

$$(A^{-1})_{jk} = \sum_{i=1}^{G} \frac{(V_{ji} V_{ki})}{(w_i)^2}. \qquad (10)$$

Using singular-matrix decomposition, we can solve the singularity problem. In the case of a singularity one or more of the elements of **W** is close to zero. We solve the problem by setting the corresponding elements in $\mathbf{W}^{-1}$ to zero:

$$(W^{-1})_{ii} = 0 \quad \text{if} \quad W_{ii} \leq \quad \text{threshold,}$$

$$(W^{-1})_{ii} = 1/w_{ii}, \quad \text{otherwise,} \qquad (11)$$

where

$$\text{threshold} = \epsilon \times (\text{maximum value of } w_{jj}|_{i=1}^{G}),$$

$$\epsilon = \text{machine accuracy.}$$

To identify the gases that cause the singularity problems, one should look at the matrices **W** and **V**; if $W_{ii} \leq$ threshold and $V_{ij} \geq \epsilon$, then j is one of the gases that gives rise to singularity.

6. Trace-Gas Flows for Biological Measurements

Experiments were performed on the trace-gas release of cherry tomatoes under anaerobic and aerobic conditions with the arrangement shown in Fig. 1. We obtained the change in conditions by admitting O_2 to a N_2 flow either before (aerobic) or after (anaerobic) the cuvette containing the tomato. In this way the N_2/O_2 gas composition that entered the photoacoustic cell left the resonance conditions for the photo-
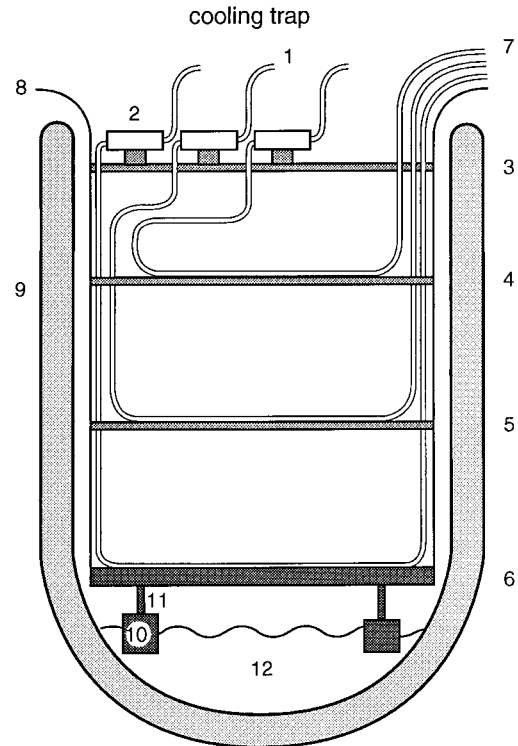

Fig. 2. Cooling trap: 1, entrance of trace gases; 2, water-vapor deposit tubes; 3, 4, and 5, aluminum plates (5 mm thick) at temperatures of 255, 200, and 150 K; 6, brass plate (20 mm thick) kept at 100 K; 7, outlet of trace gases toward the triple photoacoustic cell; 8, Teflon jacket to avoid temperature changes at the aluminum plates during refilling caused by evaporating cold N_2 vapor; 9, Dewar (200-mm inner diameter, 700-mm height); 10, aluminum block at liquid-N_2 temperature; 11, thermally isolated connection between the block and the brass plate to keep a constant temperature gradient; 12, liquid-N_2 reservoir.

acoustic cell unchanged. The O_2 flow was first led over a catalyst consisting of aluminum oxide pellets maintained at 773 K. All the hydrocarbons were then converted to H_2O and CO_2. Since among other gases our interest concerns the CO_2 release from the tomatoes, CO_2 was removed by a scrubber of potassium hydroxide (KOH) pellets before the gas was led to the sampling cuvette. After O_2 was admitted to the N_2, the total flow rate was 6 l/h. As tubing material between the sample cell and the resonator, Teflon was employed to minimize the adsorption effect of, e.g., H_2O.

Spectral selectivity is aided by the selective trapping of gases with various vapor pressures. For that purpose the trace-gas flow from the sample was split into three parts. The flows were led over different temperature levels of a cooling trap (Fig. 2). The cooling trap consisted of a Dewar that contained four interconnected metal plates at a distance of 150 mm (Fig. 2). The upper three were made of aluminum, and the lowest plate was made of brass. Brass was chosen to increase the temperature stability for this level especially during the refilling of liquid nitrogen. Below the brass plate a temperature sensor triggered refilling, which took place approximately every 5 h. At the

Table 2. Partial Vapor Pressures for Several Gases at Given Temperatures

Temperature (Kelvin)	C_2H_4 Pressure (Torr)	Acetaldehyde Pressure (Torr)	CO_2 Pressure (Torr)	Ethanol Pressure (Torr)	H_2O Pressure (Torr)
100	0.3^a		$<2 \times 10^{-4a}$		
120	10.5^b	$<1 \times 10^{-4c}$	0.03^a		
150	206.3^b	0.01^c	6.0^b	$<1 \times 10^{-5c}$	$<1 \times 10^{-6c}$
200	3420^b	2.5^c	1163^b	0.01^c	1.5×10^{-3b}

Vapor pressures were obtained from a, Ref. 18; b, Ref. 17; and c, estimated from Ref. 17.

bottom of the Dewar four aluminum blocks, connected through thin brass connections to the brass plate, kept the brass plate at a constant temperature slightly above the liquid-nitrogen temperature. The temperature stability was augmented by three control units containing a temperature sensor and a heater at the plates. The temperatures of the plates remained constant within 1 K during refilling. Only the top level was not temperature controlled, and a change of temperature of 10 K was observed during refilling. This level at a temperature of 253 K served to take out the major portion of water vapor. The diameter of the tubing at this part of the trap was increased to 8 mm, thereby providing space for the water vapor to be deposited in the form of ice. This part of the cooling trap was easily accessible; it could be cleaned every day.

All three flows from the sample first passed the top level and were then led to the different cooling levels of the trap that separated the gases by their partial vapor pressures (Table 2).[17,18] Flow 1 (100 K) was led over the lowest level of the cooling trap; next to the remaining water vapor ethanol and acetaldehyde were also frozen out; ethylene could pass the trap. CO_2, which could be produced by the tomato in relatively large amounts, might have obstructed the flow at the lowest stage. Therefore it was removed by KOH before this level of the cooling trap was entered (Fig. 1). The flow that passed through at a temperature of 150-K residual water vapor and ethanol was ideally reduced to concentrations of approximately 40 pptv and 3 ppbv, whereas acetaldehyde, ethylene, and CO_2 could pass freely at a level of parts per million in volume. At the third level (200 K) ethanol could pass and only residual water vapor was taken out. The tubes inside the Dewar leading to the different cooling levels could have become obstructed by ice after some time (approximately two days). Each level therefore contained two spare tubes that could be connected without defrosting the trap. After operation for a week the trap was warmed up to clear the trace-gas flows.

7. Gas Exchange of Cherry Tomatoes under Aerobic–Anaerobic Conditions

Physiological processes in plant tissue often occur simultaneously with characteristic gas releases into the atmosphere. Their study requires a fast analysis of the concentration of these gases in the air surrounding, e.g., a fruit under investigation. Our choice was the tomato; specifically, its induced and interrupted fermentation were addressed by means of measuring ethanol, acetaldehyde, ethylene, and CO_2 releases simultaneously.

During normal aerobic ripening of tomatoes physiological processes are marked by the release of gases. The most famous is the increase of ethylene emission during ripening accompanied by a less pronounced CO_2 emission attributed to enhanced respiration of the fruit.[19] The maximum respiration is observed while the fruit is between its mature-green and orange stages. Thereafter the decay of CO_2 emission is consistent with the loss of firmness and the production of ethanol.

The pathway by which, next to other gases, ethylene leaves a tomato (for approximately 90% through the stem-scar region) has been addressed in a number of careful investigations.[20] Since the gas acts as a hormone, already at low concentrations it induces changes in plants: ripening, growth, seed germination, abscission, and senescence are influenced. Oxygen is needed to produce C_2H_4 from its precursor 1-aminocyclopropane-1-carboxylic acid (ACC). Without an oxygen supply, endogenous ethylene production cannot take place during the last step in the biosynthesis of ethylene.

Normal respiration involves oxidation of glucose to release energy needed for the maintenance and development of the biological material ($C_6H_{12}O_6 + 6O_2 \rightarrow 6CO_2 + 6H_2O$ + energy). In the absence of oxygen the complete oxidation of sugar molecules is prevented and the plant recovers the necessary energy from sugars by fermentation, starting with glucose ($C_6H_{12}O_6$) and converting to pyruvate ($CH_3COCOOH$) and acetaldehyde (CH_3COH) and finally to ethanol (CH_3CH_2OH) (see, e.g., Ref. 21). The efficiency of this process, however, is extremely low: only 2.5% compared with normal respiration.

Anaerobic conditions occur in nature, e.g., during flooding, the first hours of seed germination, and ripening of bulky fruit. Most plants are able to adapt to short anaerobic periods. Long periods, however, are fatal to the majority of higher plants. The accumulation of fermentation products (lactate, acetaldehyde, and ethanol) is considered to be an important factor that defines the degree of plant tolerance for anaerobic conditions.

Anaerobic conditions lead to fermentation, which provides the fruit with energy, although less efficiently than through normal aerobic respiration. Restored normal oxygen levels permit respiration again. However, the reentering oxygen finds a to-

mato that has accumulated ethanol at high concentrations. This fact leads to postanaerobic processes that in extreme cases can cause the destruction of cell membranes and cell death.[22]

Measurements were performed on cherry tomatoes from Israel (Carmel–Sulat) at light conditions. These tomatoes were without coronet, of light-red color, and of good firmness (7 g of average fresh weight). Corrected for flow rate and fresh weight, the measured concentrations (Figs. 3 and 4) led to production rates for which 1-ppbv gas concentration corresponded to 36 pmol/h/g fresh weight. Selection of the laser lines for multicomponent measurements on tomatoes was performed by use of the data in Table 1. For the multicomponent calculation and the error analyses the laser lines indicated with a superscript a were taken into account.

The effects of applying anaerobic conditions 3 h after placing three cherry tomatoes in the cuvette are shown in Fig. 3. The switch from air (80% N_2 + 20% O_2) to N_2 resulted in changes in the tomato metabolism that were manifested by changes in the production rates of the measured gases. As expected, the ethylene production decayed (from 9 ppbv to below our detection limit). Ethylene production cannot take place without an oxygen supply. Oxygen is needed for the last stage of ethylene biosynthesis (from ACC to C_2H_4).[19] The observed decay of ethylene production was therefore determined by oxygen consumption within the tissue (e.g., respiration) and by oxygen and ethylene diffusion out of the tissue. The decay of C_2H_4 production within 0.5 h of the onset of anaerobic conditions is in agreement with previous results.[7,14]

During the anaerobic period the ethanol concentration rose continuously; after 10 h the increase was sevenfold from 100 to 700 ppbv. The acetaldehyde concentration rose at a much slower rate, reaching 6 ppbv after 10 h. Within our detection limit (0.1 ppbv) we did not detect acetaldehyde at normal aerobic conditions. Our measurements show a nearly linear increase in ethanol production starting within 1 h after the onset of anaerobic conditions. This rise indicates a switch to ethanolic fermentation within the tomato. Acetaldehyde was emitted with a similar delay; it became detectable (0.1 ppbv) 3.5 h directly after the change to anaerobic conditions (Fig. 3). The low and constant acetaldehyde–ethanol ratio during anoxia suggests a rapid and efficient conversion of acetaldehyde to ethanol, thus avoiding the accumulation of toxic metabolite acetaldehyde.

CO_2 production slowly decreased from 2 ppmv to below 1 ppmv during the anaerobic period (data not shown). Anaerobic oxidation of 1 mole of glucose to ethanol produced three times less CO_2 than aerobic respiration. Often the production of CO_2 by plant tissue is not lowered by anaerobic conditions. This is a sign that glycolysis (glucose–pyruvate conversion) activity was increased at least threefold. The increase in respiration under low oxygen and anaerobic conditions, known as the Pasteur effect, is thought to play an important role in the adaptation of
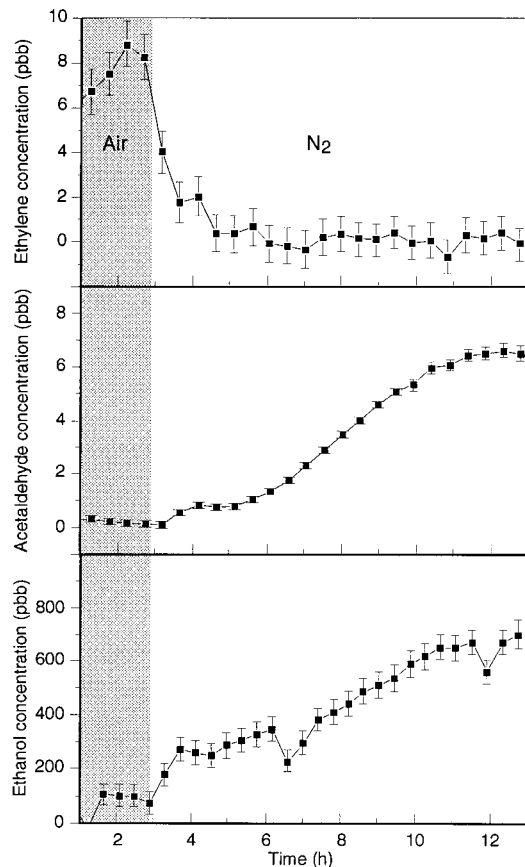

Fig. 3. Aerobic-to-anaerobic transition. At 0 h, three cherry tomatoes were placed in a cuvette with 80% N_2 + 20% O_2 flow; at 3 h, O_2 flow was switched from the entrance to the exit port of the cuvette, resulting in anaerobic conditions. We obtained each data point shown by subtracting the respective gas concentration calculated for the empty cuvette from that for the tomato cuvette.

plants to anaerobic conditions.[23] As shown (also in Fig. 4), the difference in CO_2 emission was negligible instead by a factor of 3, representing indeed an increased rate of glycolysis.

The difficulty in comparing our results with those found in the literature is due to the inherently different measuring technique. In most of the studies relatively long incubation times are needed to reach the detection limit of gas chromatography (approximately 1 ppmv for acetaldehyde and 50–100 ppbv for ethanol); the measured values yield the integral of ethanol and acetaldehyde release, whereas our measurements yield directly the emission rate.

The error bars in Figs. 3 and 4 are calculated from the multicomponent analyses taking into account 14 laser lines (Table 1). For ethanol in particular, the error bars are much larger (50–100 ppbv) than the detection limit (10 ppbv); the latter is based on the signal-to-noise ratio at the strongest ethanol-absorbing laser line. One can reduce the error bars by taking fewer laser lines into account, but then the accuracy of the data (owing to interference from other gases) is also reduced.

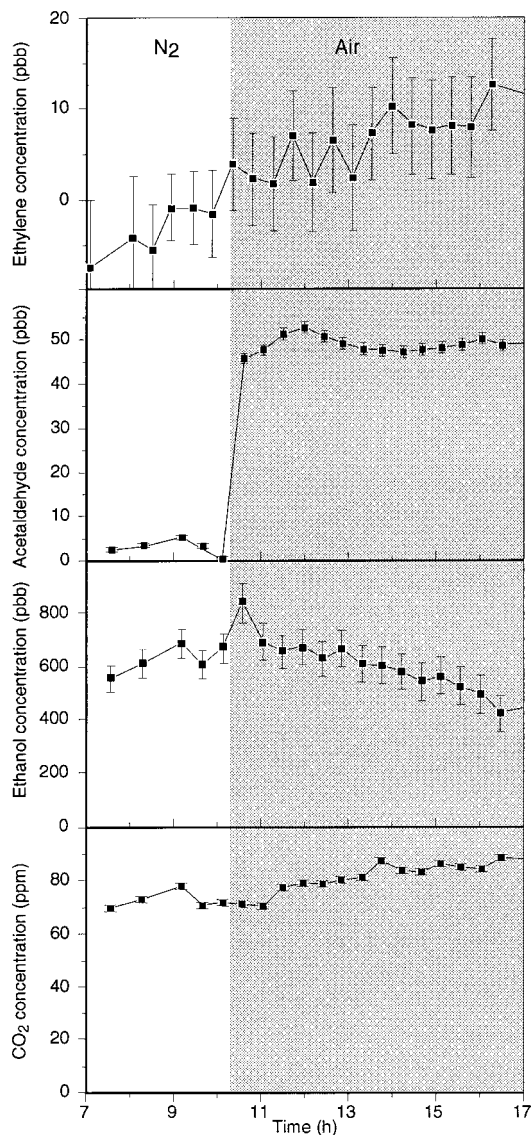The transition backward from anaerobic to aerobic

Fig. 4. Anaerobic-to-aerobic transition for a different experiment compared with Fig. 3. At 0 h, anaerobic conditions were established in a cuvette with three fresh cherry tomatoes; at 10.2 h, aerobic conditions were reinstalled.

oxygen conditions. The principal mechanism of postanoxic injury is through the highly reactive superoxide radical ($O_2{}^-$), the first intermediate in the reduction of O_2 and a precursor of other toxic intermediates. Living cells evolved mechanisms to protect themselves from oxygen toxicity. Ascorbate (Vitamin C) is an example of an antioxidant that acts as an electron acceptor and is able to scavenge free radicals. It was suggested[24] that postanoxic oxidation of anaerobically accumulated ethanol may result in an upsurge of acetaldehyde production, which in turn could have a toxic effect on the recovering tissues. Two main pathways for the oxidation of ethanol to acetaldehyde have been proposed: a fast peroxidation of ethanol by the enzyme catalase and a slow back reaction of ethanol with alcohol dehydrogenase (ADH). Our results clearly indicate the existence of a fast (<0.5 h) upsurge in acetaldehyde production as a response to the reinstallation of aerobic conditions. The fast increase in acetaldehyde after reexposure to air helped to rule out ADH as the main catalyst for the reverse ethanol-to-acetaldehyde reaction. Based on our time-resolved measurements, we estimate that a tenfold increase in acetaldehyde production can occur within <1–5 min after reexposure to air. Future experiments are planned to exploit fully the advantages of photoacoustics for a fast (30 s) time-resolved acetaldehyde detection from plant tissues.

8. Conclusions

Our triple intracavity photoacoustic cell in a liquid-nitrogen-cooled CO laser has been able to trace ethanol and acetaldehyde at a level of parts per billion in volume in a multicomponent air mixture with ethylene, CO_2, and water vapor. The time-dependent anaerobic and postanaerobic processes in tomatoes were monitored by the emission of acetaldehyde and ethanol (0.1 and 10 ppbv detection limits, respectively) during changing anaerobic and postanaerobic conditions.

References

1. J. Slanina, *Biosphere Atmosphere Exchange of Pollutants and Trace Substances* (Springer-Verlag, Berlin, 1997).
2. Z. W. Weitz, A. J. Birnbaum, P. A. Sobotka, E. J. Zarling, and J. L. Skosey, "High breath pentane concentrations during acute myocardial infarction," Lancet **337,** 933–935 (1991).
3. T. W. Kimmerer and T. T. Kozlowski, "Ethylene, ethane, acetaldehyde and ethanol production by plants under stress," Plant Physiol. **69,** 840–847 (1982).

conditions was performed with three fresh cherry tomatoes kept under 100% N_2 flow for 10 h (Fig. 4). This reexposure to O_2 caused a small increase of ethylene production from below the detection limit to 10 ppbv. Acetaldehyde showed more than a tenfold increase of concentration to 50 ppbv within 15 min and decreased only slowly during the following hours. Ethanol response was less pronounced: the emission decreased steadily after the onset of aerobic conditions, and this was probably due to the formation in the tissue of liquid ethanol, which evaporates only slowly at room temperature.

The postanaerobic effect (postanoxic) is well documented in human and animal systems. In plants injury caused by postanoxic effects can occur under natural conditions following flooding, soaking of seeds, and exposure to air of fruit stored under low

4. M. W. Sigrist, *Air Monitoring by Spectroscopic Techniques* (Wiley, New York, 1994).

5. R. T. Jongma, M. G. H. Boogaarts, I. Holleman, and G. Meijer, "Trace gas detection with cavity ring down spectroscopy," Rev. Sci. Instrum. **66,** 2821–2828 (1995).

6. F. J. M. Harren, F. G. C. Bijnen, J. Reuss, L. A. C. J. Voesenek, and C. W. P. M. Blom, "Sensitive intracavity photoacoustic measurements with a CO_2 waveguide laser," Appl. Phys. B. **50,** 137–144 (1990).

7. H. S. M. de Vries, F. J. M. Harren, L. A. C. J. Voesenek, C. W. P. M. Blom, E. J. Woltering, H. C. P. M. van der Valk, and J. Reuss, "Investigation of local ethylene emission from intact Cherry tomatoes by means of photothermal deflection and photoacoustic detection," Plant Physiol. **107,** 1371–1377 (1995).

8. S. B. Tilden and M. Bonner Denton, "A comparison of data reduction techniques for line excited optoacoustic analysis of mixtures," Appl. Spectrosc. **39,** 1017–1022 (1985).

9. P. L. Meyer and M. W. Sigrist, "Atmospheric pollution monitoring using CO_2-laser photoacoustic spectroscopy and other techniques," Rev. Sci. Instrum. **61,** 1779–1807 (1990).

10. S. Bernegger and M. W. Sigrist, "CO laser photoacoustic spectroscopy of gases and vapors for trace gas analysis," Infrared Phys. **30,** 375–429 (1990).

11. W. Urban, in *Frontiers of Laser Spectroscopy of Gases*, A. C. P. Alves, J. M. Brown, and M. Hollas, eds., Vol. 234 of NATO Advanced Studies Institute Series (Kluwer Academic, Dordrecht, The Netherlands, 1988), pp. 9–42.

12. T. C. Lioutas, "Challenges of controlled and modified atmosphere packaging: a food company's perspective," Food Technol. **42,** 78–86 (1988).

13. F. G. C. Bijnen, F. J. M. Harren, J. H. P. Hackstein, and J. Reuss, "Intracavity CO laser photoacoustic trace gas detection: cyclic CH_4, H_2O, and CO_2 emission by cockroaches and scarab beetles," Appl. Opt. **35,** 5357–5368 (1996).

14. F. G. C. Bijnen, J. Reuss, and F. J. M. Harren, "Geometrical optimization of a longitudinal resonant photoacoustic cell for sensitive and fast trace gas detection," Rev. Sci. Instrum. **67,** 2914–2923 (1996).

15. A. Thöny and M. W. Sigrist, "New developments in CO_2 laser photoacoustic monitoring of trace gases," Infrared Phys. Technol. **36,** 585–615 (1995).

16. W. H. Press, *Numerical Recipes in C*, 2nd ed. (Cambridge U. Press, Cambridge, UK, 1992).

17. D. R. Lide, *Handbook of Chemistry and Physics*, 73rd ed. (CRC Press, Boca Raton, Fla., 1992), pp. 6-69–6-99.

18. A. W. Tickner and F. P. Lossing, "Measurements of low vapor pressures," J. Phys. Chem. **55,** 733–738 (1951).

19. F. B. Abeles, P. W. Morgan, and M. E. Saltveit, Jr., *Ethylene in Plant Biology*, 1st ed. (Academic, San Diego, Calif., 1992).

20. H. S. M. de Vries, M. A. J. Wasono, F. J. M. Harren, E. J. Woltering, H. C. P. M. van der Valk, and J. Reuss, "Ethylene and CO_2 emission rates and pathways in harvested fruits investigated, *in situ*, by laser photodeflection and photoacoustic techniques," Postharvest Biol. Technol. **8,** 1–10 (1996).

21. F. B. Salisbury and C. W. Ross, *Plant Physiology* (Wadsworth, Belmont, Calif., 1992).

22. P. Perata and A. Alpi, "Ethanol induced injuries to carrot cells, the role of acetaldehyde," Plant Physiol. **95,** 748–752 (1991).

23. W. Armstrong, R. Brändle, and M. B. Jackson, "Mechanisms of flood tolerance in plants," Acta Bot. Neerl. **43,** 307–358 (1994).

24. L. S. Monk, R. Brändle, and R. M. M. Crawford, "Catalase activity and post-anoxic injury in monocotyledonous species," J. Exp. Bot. **38,** 233–246 (1987).